Preprints of the 21st IFAC World Congress (Virtual)
Berlin, Germany, July 12-17, 2020

Real-Time Optimized Model Predictive Control of an Active Roll Stabilization System with Actuator Limitations

Georgi Nareyko,* Patrick Biemelt,**
Ansgar Trächtler**

*Dr. Ing. h.c. F. Porsche AG, 71287 Weissach, Germany,
(e-mail: georgi.nareyko@porsche.de).
**Chair of Control Engineering and Mechatronics, Heinz Nixdorf Institute, University of Paderborn,
Germany (e-mail: [patrick.biemelt, ansgar.traechtler]@hni.uni-paderborn.de).

Abstract: Active roll stabilization systems are used to improve both the ride dynamics and ride comfort. For that, the measureable information about road disturbance should be used to calculate the control variable for the actuators at the front and rear axle. Even without previewed disturbance information the whole car dynamics can be modelled and provide future states of the controlled system which consequently can be regarded in the calculation in advance. By the framework of a Model Predictive Control, the actuator limitations can be included. Additionally, the movement of the car body and each wheel is regarded, so that an optimal allocation of the control variables on both actuators takes place. With both aspects, namely the actuator limitations and the optimization itself, a high potential for ride comfort improvement is generated.

Keywords: Active vehicle suspension, Actuator limitations, Model Predictive Control, Optimization, Ride comfort, Vehicle dynamics.

1. INTRODUCTION

In this work, the focus is set on using the Model Predictive Control (MPC) to show up the ride comfort improvement potential if a short prediction horizon and actuator limitations are considered within the control design. The usage of MPC in context of ride comfort has already been evaluated in several publications.
Cho (1999), Cho et al. (2005) and Göhrle (2013) analyzed the implementation of a MPC with available preview information using a camera to scan the road in front of the vehicle. By that, the future road disturbance could be roughly predicted. The optimal actuator set variables were thereby calculated in advance. However, a challenge arises if this preview information is not available, has a poor quality or is slowly updated. Further works from Canale et al. (2006), Giorgetti et al. (2006) and Nguyen et al. (2016) presented a method which did not require preview information to control a semi-active suspension of a car. However, an in-depth analysis or application with an active stabilization system has not been realized yet.

Both, the driving dynamics and the ride comfort, are essential design targets in the chassis development process. To influence the roll mode, which means the rotation around the longitudinal axis of the car body, an electromechanical active roll stabilization is used. For that, two almost equal actuators are installed at the front and rear axle. As shown in Fig. 1 the actuator connects both halves of the anti-roll bars. The analyzed system is constructed with a BLDC Motor and a three-stage planetary gear to provide high torques. The system components have been presented by Illg et al. (2018). Regarding the driving dynamics, the impact of road excitation on the roll mode is essential. On the one hand, the force is transmitted by the wheels to the car body. On the other hand, by torsion of the stabilizer bar, an additional force is set.

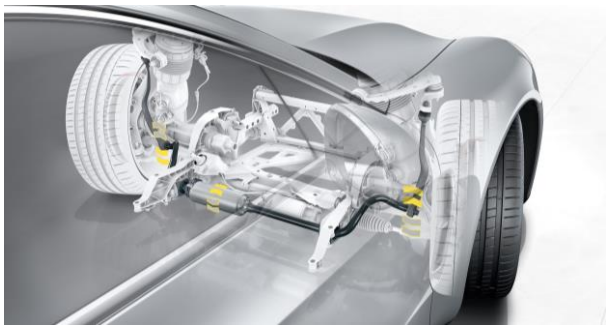

Fig. 1. Electromechanical active roll stabilization at the front axle of a vehicle.

This additional force can be influenced by the angle of the actuator as the force results from the difference of the external (caused by relational wheel deflection) and the actuators' rotational angle. The set torque is transferred as reaction forces by the coupling rods on both wheel suspensions to the vehicle body. Several boundary conditions should be regarded for control design. That includes a limited bandwidth of the actuator and the limitations shown in Table 1.

Table 1. Actuator limitations

Description	Value
Gear transmission ratio i_{gear}	1:191
Torque limit $\pm Tq_{max}$	8 Nm
Rotational speed limit n_{max}	400 rad/sec

As the transmission ratio of the three-stage planetary gear is i_{gear}=191, the torque is hugely increased while the maximum rotational speed drops to ~2.08 rad/s. The dynamics of the actuator can be idealized to a second order lag element with a bandwith of 10 Hz. Within control design, not only the ride comfort improvement and actuator limitations should be respected, but also the real-time capability. As already stated, one disadvantage of the MPC is the high computational demand as the optimization takes place in every step and includes multiplication of several matrices with higher dimensions. In order to fulfill the real-time capability, the limit for computational time is set to 2.5 ms, which represents a realistic ECU limit.

2. VEHICLE SYSTEM MODEL

2.1 State Space Model Equations

A linear vertical car model is used to describe the controlled system. It is formed by model equations for the seven degrees of freedom, which are: body roll angle φ_a, every translational wheel travel z_{Rij} and actuator angle $\varphi_{akt,i}$ at the front and rear axle as shown in Fig. 2. Body heave and pitch angle are already eliminated. It can be shown, that in a linear model both do not affect the roll model, as the affected vertical force variation drops out of the roll mode.

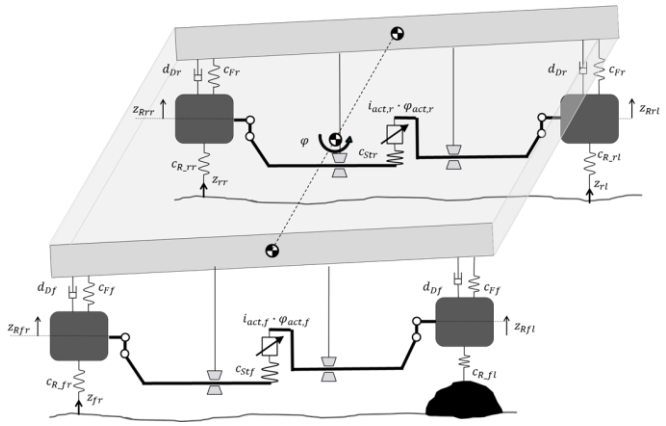

Fig. 2. Vehicle model with seven degrees of freedom, Nareyko (2019)

For each quarter-car the wheel is modelled as a spring stiffness between wheel and road unevenness z_{ij}. Forces between wheel and car body are composed of three components, namely damper, spring and stabilizer bar forces F_{Sti}. The equations are briefly shown in (1). The forces are separated by front/rear.

$$\Theta_{A,x}\ddot{\varphi} = \frac{b_f}{2}\left(-F_{fl} + F_{fr}\right) + \frac{b_r}{2}\left(-F_{rl} + F_{rr}\right) \tag{1}$$

$$F_{fl} = c_{Ff}\left(\frac{b_f}{2}\varphi - z_{Rfl}\right) + d_{Df}\left(\frac{b_f}{2}\dot{\varphi} - \dot{z}_{Rfl}\right) - F_{Stf}$$

$$F_{fr} = c_{Ff}\left(-\frac{b_f}{2}\varphi - z_{Rfr}\right) + d_{Df}\left(-\frac{b_f}{2}\dot{\varphi} - \dot{z}_{Rfr}\right) + F_{Stf}$$

$$F_{rl} = c_{Fr}\left(\frac{b_r}{2}\varphi - z_{Rrl}\right) + d_{Dr}\left(\frac{b_r}{2}\dot{\varphi} - \dot{z}_{Rrl}\right) - F_{Str}$$

$$F_{rr} = c_{Fr}\left(-\frac{b_r}{2}\varphi - z_{Rrr}\right) + d_{Dr}\left(-\frac{b_r}{2}\dot{\varphi} - \dot{z}_{Rrr}\right) + F_{Str}$$

$$F_{Stf} = c_{Stf}(z_{Rfl} - z_{Rfr} - b_f\varphi + i_{act,f}\varphi_{act,f})$$

$$F_{Str} = c_{Str}(z_{Rrl} - z_{Rrr} - b_r\varphi + i_{act,r}\varphi_{act,r})$$

Kinematic factors are already included in the stiffness and damper rates so that the wheel related value is used. That means, the real components' stiffness and damper rate was initially related to its chassis linking point but is transformed to its effective value above the wheel center. Additionally used parameters are the track width b, body spring stiffness c_F, body damper rate d_D and stabilizer bar stiffness c_{St}. The wheels' movement equations are also part of the model but not displayed in (1). Similar models may be found in Koletzko (2008) or Nguyen et al. (2016). Additionally, the actuator dynamics is modelled as a second order lag element element with a bandwidth of 10Hz as shown in (2).

$$\ddot{\varphi}_{act} = -\frac{\varphi_{act}}{T_{act}^2} - \frac{2D_{act}\dot{\varphi}_{act}}{T_{act}} + \frac{\varphi_{act,set}}{T_{act}^2} \tag{2}$$

In this case we assume $T_{act} = 0.0159$ and $D_{act} = 0.708$.

Summing up the equations, a state space model is created as displayed in (3)

$$\dot{x}(t) = \tilde{A}x(t) + \tilde{B}_u u(t) + \tilde{B}_z z(t)$$

$$y(t) = \tilde{C}x(t)$$

with

$$x = \left[\varphi, z_{Rfl}, z_{Rfr}, z_{Rrl}, z_{Rrr}, \varphi_{act,f}, \varphi_{act,r}, \dot{\varphi}, \dot{z}_{Rfl}, \dot{z}_{Rfr}, \dot{z}_{Rrl}, \dot{z}_{Rrr}, \dot{\varphi}_{act,f}, \dot{\varphi}_{act,r}\right]^T \tag{3}$$

$$u = \left[\varphi_{act,set,f}, \varphi_{act,set,r}\right]^T$$

$$z = \left[z_{fl}, z_{fr}, z_{rl}, z_{rr}\right]^T.$$

They are discretized subsequently

$$x_{k+1} = A \cdot x_k + B_u \cdot u_k + B_z \cdot z_k$$

$$y_k = C \cdot x_k \tag{4}$$

with $u_k \in \mathbb{R}^m$, $x_k \in \mathbb{R}^n$, $z_k \in \mathbb{R}^p$ and $y_k \in \mathbb{R}^r$. So far the model was designed to determine the current system output y_{k+1} only one step ahead. As a preparation for the model predictive control the matrices will be extended for a time horizon of n_p so that the matrices

$$\hat{u} = [u_k, \dots, u_{k+n_p-1}]^T \in \mathbb{R}^{mn_p \times 1}$$

$$\hat{y} = [y_{k+1}, \dots, y_{k+n_p}]^T \in \mathbb{R}^{rn_p \times 1} \tag{5}$$

are introduced.

Enhancing (4) for every time step $[1, \dots, n_p]$, it leads to the final model equation in (6).

This basic formulation is also shown in Maciejowski (2002), Adamy (2009), Ilmer (2019) and was applied e.g. by Göhrle (2013).

$$\hat{y} = \mathcal{F}x_k + \mathcal{H}\hat{u} \tag{6}$$

$$\mathcal{F} = \begin{bmatrix} CA \\ CA^2 \\ \vdots \\ CA^{n_p} \end{bmatrix} \in \mathbb{R}^{rn_p \times n}$$

$$\mathcal{H} = \begin{bmatrix} CB & 0 & \dots & 0 \\ CAB & CB & 0 & 0 \\ \vdots & \vdots & \ddots & 0 \\ CA^{n_p-1}B & CA^{n_p-2}B & \dots & CB \end{bmatrix} \in \mathbb{R}^{rn_p \times mn_p}$$

Enhancing (6) by an additional disturbance input from an observer leads to (7)

$$\hat{y} = \mathcal{F}x_k + \mathcal{H}_u\hat{u} + \mathcal{H}_z\hat{z} \tag{7}$$

with $\mathcal{H}_u = \mathcal{H}$, while $\mathcal{H}_z$ has a similar structure but only contains $B_z \in \mathbb{R}^{n \times p}$ instead of $B \in \mathbb{R}^{m \times p}$.

3. MODEL PREDICTIVE CONTROLLER

3.1 Optimization Problem

The quadratic cost function to be minimized within the prediction horizon is defined as

$$J = \sum_{i=1}^{n_p} \left(y_{Ref,k+i} - Cx_{k+i}\right)^T Q_i \left(y_{Ref,k+i} - Cx_{k+i}\right) + \sum_{i=0}^{n_p-1} u_{k+i}^T R_i u_{k+i} \tag{8}$$

with the dimensions $C \in \mathbb{R}^{r \times n}, Q_i \in \mathbb{R}^{r \times r}$ and $R_i \in \mathbb{R}^{m \times m}$. To determine the optimal solution it is firstly rewritten to

$$J = (\hat{y} - y_R)^T Q (\hat{y} - y_R) + \hat{u}^T R \hat{u}. \tag{9}$$

By that, the dimensions change to $Q \in \mathbb{R}^{rn_p \times rn_p}$ and $R \in \mathbb{R}^{mn_p \times mn_p}$ and the diagonal axis contains the values of Q_i and R_i, respectively. Then, if there are no constraints considered, inserting (6) for $\hat{y}$ and setting $y_R = [0 \dots 0]^T$, the solution is determined by partly derivation. It leads to

$$(H^T Q H + R)\hat{u} + H^T Q F x_k = 0 \tag{10}$$

and respectively

$$\hat{u} = -(H^T Q H + R)^{-1} H^T Q F x_k. \tag{11}$$

That is also shown in Adamy (2009) and Maciejowski (2002). As a result $\hat{u}$ contains set variables for the whole prediction horizon. However, only the first $\hat{u}_k$ for the current time step is used. The optimiziation is exectued subsequently for the next time step.

With regard to the vehicle system model from section 2 the control structure is shown in Fig. 3.

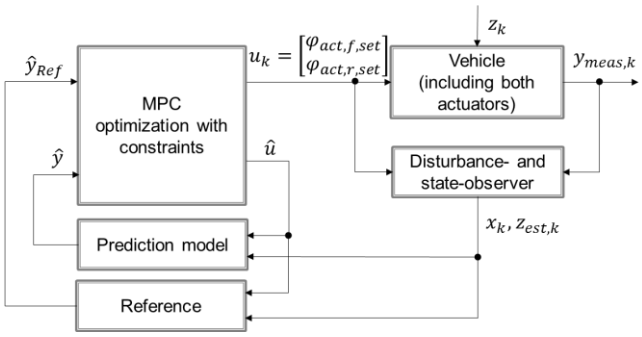

Fig. 3. Control structure with actuator, disturbance observer, prediction and optimization model.

The disturbance and state observer are not part of this contribution and therefore not described in-depth. So, x_k and $z_{est,k}$ are available with a certain accuracy. Further, the predicted system output $\hat{y}$ is calculated with the current state x_k and input vector $\hat{u}$ over the time horizon n_p. Afterwards, the optimization towards a reference state $\hat{y}_{Ref}$, which is set to zero in this case, is implemented. Constraints are an essential part within the optimization problem. due to their impact, they are described separately in section 3.2.

3.2 Actuator Limitations

The constraints were formed based on the displayed actuator limitations in section 1. The non-linear actuator may only be approximated as a PT2 up to a certain limit. The working range is sketched in Fig. 4.

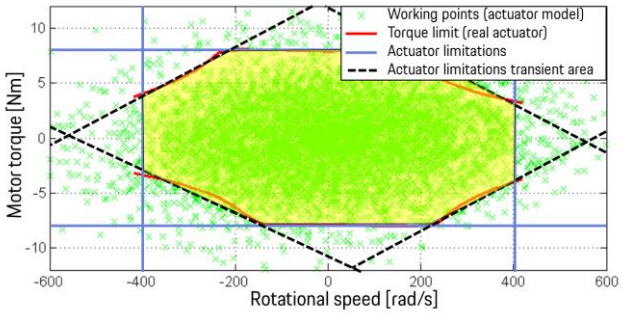

Fig. 4. Working range of the BLDC Motor and approximated limitations

As the motor and not the whole actuator is regarded towards its constraints, the gear transmission ratio i_{gear} is only considered afterwards. Compared to the real working range there are two variants of assumption. The first variant assumes a constant limit of torque and rotational speed while the second variant approximates a transient area by a linear function. The cause for the transient area is the decreasing torque at rotational speed above the nominal speed. Also the power as a product of torque and rotational speed is fixed to a maximum limit which can be deduced from the slope in the transient area.

For the purpose of limiting the rotational speed, it is defined as the systems' output for the whole prediction horizon which slightly changes (6) to (12):

$$\hat{y}_{act} = \mathcal{F}_{act} x_{act,k} + \mathcal{H}_{act} \hat{u};\ \hat{y}_{act} \in \mathbb{R}^{sn_p \times 1} \tag{12}$$

The second constraint, namely the torque limit, is firstly converted into a corresponding maximum angular acceleration

$$a_{max} = Tq_{max} t_s / \Theta \tag{13}$$

with sample time t_s and inertia moment Θ which equals T_{act}^2 from (2). Secondly, by introducing the matrix

$$\mathcal{M} = \begin{bmatrix} I & 0 & \dots & 0 \\ -I & I & \dots & 0 \\ \vdots & \ddots & \ddots & \vdots \\ 0 & \dots & -I & I \end{bmatrix} \in \mathbb{R}^{(sn_p \times sn_p)}, \tag{14}$$

the angular acceleration is supposed to be the change of rotational speed within two time steps.

Altogether, the complete optimization problem with constraints can now be formulated as in (15)

$$\min_{\hat{u}} J = (\hat{y} - y_R)^T Q (\hat{y} - y_R) + \hat{u}^T R \hat{u} \tag{15}$$

$$\text{s.t. } -n_{max} \leq \mathcal{F}_{act} x_{act,k} + \mathcal{H}_{act} \hat{u} \leq n_{max}$$

$$-a_{max} \leq \mathcal{M}\mathcal{F}_{act} x_{act,k} + \mathcal{M}\mathcal{H}_{act} \hat{u} \leq a_{max}$$

Taking up Fig. 4, one last step is missing. The transient area leads to further constraints which will be only depicted shortly. Using a linear equation the maximum torque

$$Tq_{max,i} = m_{slope} \dot{\varphi}_{act,i} + m_{offset}\ \forall\ i \in [1, \dots, n_p] \tag{16}$$

is depending of the current rotation speed. The fixed values for m_{slope} and m_{offset} can be calculated using the grid points in Fig. 4. Afterwards it may be inserted in (13) and then in (15) to obtain an enhanced optimization problem with eight constraints instead of four. A valuation has been carried out by Ilmer (2019).

3.3 Optimization Goal

The output vector $y_{k+i} = C x_{k+i}$ for $i = 1, \dots, n_p$ may be assumed freely according to the minimization goals. As the roll mode of the vehicle is of importance it is set to

$$y_{k+i} = [\varphi\ \dot{\varphi}\ \ddot{\varphi}]^T = C x_{k+1}. \tag{17}$$

The roll angle and roll rate correspond to the system states. As the roll acceleration is not part of the system states it is calculated by linear combination of the corresponding line in the system matrix A. By setting the entries of the diagonal positive definite matrix $Q \in \mathbb{R}^{rn_p \times rn_p}$ and $R \in \mathbb{R}^{mn_p \times mn_p}$ the weighting between energy and ride comfort is determined. There is no calculation rule how to determine these matrices. An efficient way has been displayed by Nareyko et al. (2019). Therefore, the system is excited by a measured road disturbance on a ride comfort test track. The roll acceleration spectrum is divided into three significant areas which are 1 – 3 Hz (car body eigenfrequency), 4 – 8 Hz (human sensitive eigenfrequency) and 11 – 16 Hz (wheel eigenfrequency). The weighting of φ, $\dot{\varphi}$, or $\ddot{\varphi}$ affects these areas differently and may be evaluated by characteristic values which take into account the maximum values and the integral of the frequency spectrum areas.

The solution of the optimization problem (15) may be found using a toolbox such as *mpcqpsolver* for *MATLAB* which is based on the algorithm by Biegler et al. (1993,1994).

3.4 Move Blocking Strategy

In order to reduce the required computational effort for solving the optimal control problem (15) and thus realize a further prediction horizon, the approach of *Move Blocking* is presented subsequently. Thereby, the basic idea is to determine the optimal control variables $u_{k+i}\ \forall\ i \in [0, \dots, n_p - 1]$ only for defined time steps within the moving horizon, since the computational complexity is directly linked to the number of optimization variables (Cagienard et al., 2007). All other actuating variables are fixed and therefore do not represent free inputs. In this context, the concept of *Delta Input Blocking* (DIB) is introduced, in which the rate of change Δu_{k+i} is kept constant between predefined actuating variables. The fixed optimization variables are thus determined by a linear interpolation between the optimized actuating variables. For this purpose, the process model according to (4) is initially formulated as a function of the change in the actuating variables. The relation $u_k = u_{k-i} + \Delta u_k$ leads to the system description

$$\begin{aligned} x_{k+1} &= A \cdot x_k + B_u \cdot u_{k-1} + B_u \cdot + \Delta u_k + B_z \cdot z_k \\ y_k &= C \cdot x_k\ . \end{aligned} \tag{18}$$

Referred to Maciejowski (2002), using this linear state space description, all future state variables $x_{k+i}\ \forall\ i \in [1, \dots, n_p]$ within the prediction horizon are described as a function of the new optimization variables

$$\Delta \hat{u} = \begin{bmatrix} \Delta u_k \\ \vdots \\ \Delta u_{k+n_p-1} \end{bmatrix}. \tag{19}$$

Following the concept of the DIB, defined elements of the vector $\Delta \hat{u} \in \mathbb{R}^{p \cdot n_p}$ are fixed in the numerical optimization, which leads to new optimization variables $\Delta \tilde{u} \in \mathbb{R}^{p \cdot n_B}$ with $n_B \leq n_P$. For this, the transformation

$$\Delta \hat{u} = (T \otimes I) \cdot \Delta \tilde{u} \tag{20}$$

is introduced. Here, the operator $\otimes$ describes the *Kronecker product* and I the uniform matrix of dimension p. The fixed elements of the actuating variable changes are defined by the so-called *Blocking Matrix* $T \in \mathbb{R}^{n_P \times n_B}$, which is a matrix of ones and zeros only that exactly contains one non-zero element in each row. In order to explain the general idea of this approach in detail, an optimization problem with a prediction horizon of $n_P = 4$, thus $4p$ optimization variables, is

considered as an example. If the transformation according to (20) is performed with

$$T = \begin{bmatrix} 1 & 0 \\ 1 & 0 \\ 1 & 0 \\ 0 & 1 \end{bmatrix}, \tag{21}$$

the actuating variable changes Δu_{k+1} and Δu_{k+2} are kept constant and $\Delta u_k = \Delta u_{k+1} = \Delta u_{k+2}$ applies. The new optimization variables are now defined by $\Delta\tilde{u} = [\Delta u_k^T \quad \Delta u_{k+3}^T]^T$, reducing the number of actuating variable changes to be optimized from $4p$ to $2p$. With this approach, larger prediction horizons can be considered without significantly increasing the number of optimization variables. However, it should be noted that the solution to the original optimal control problem (15) is not always found, especially if the number of optimization variables is significantly reduced. The application of the proposed strategy leads in the context of this paper to the modified cost function:

$$J = \sum_{i=1}^{n_p} \left(y_{Ref,k+i} - Cx_{k+i}\right)^T Q \left(y_{Ref,k+i} - Cx_{k+i}\right) + \sum_{i=0}^{n_B} \Delta\tilde{u}_{k+i}^T \cdot R \cdot \Delta\tilde{u}_{k+i} \tag{22}$$

In analogy to (8), the solution of the resulting optimization problem achieves an increase in driving comfort by minimizing the roll acceleration. In addition to the system equations (18), the constraints were also formulated as a function of $\Delta\tilde{u}$ to ensure that the physical limits of the actuators are respected at all times. The corresponding Blocking Matrix T was selected in such a way that a prediction horizon of $n_P = 50$ is realized with the same number of $10p$ optimization variables. While the first four actuating variable changes $\Delta u_k, \ldots \Delta u_{k+3}$ are optimized without using Move Blocking, all remaining optimization variables in (22) are equidistantly distributed over the remaining prediction horizon. The intermediate actuating variables are fixed according to the idea of the DIB. Thus, it is possible to meet the real-time requirements with a similar sampling rate, although the prediction horizon has been extended from $n_P = 10$ to $n_P = 50$.

4. SIMULATION RESULTS

To analyze the effect of the designed control, a simplified control should be firstly introduced which will be called reference control. With the current system states $\varphi, z_{Rfl}, z_{Rfr}, z_{Rrl}$ and z_{Rrr} the ride height (displacement of the wheel relatively to the car body) and thus the roll bar torsion angle is calculated by (23)

$$\varphi_{ext} = (z_{Rfl} - z_{Rfr} - b_f\varphi)/i_{act,f} \tag{23}$$

exemplarily for the front axle. The equation results assuming $F_{Stf} = 0$ from (1). Thus, the stabilizer force induced by road disturbance would be zero if there were no actuator dynamics, limitations or dead times. As this variant will not lead to satisfying results due to the named problems, the improvement potential of the designed MPC will be compared against this reference control.

A simulation of a driving maneuver on a ride comfort test track has been carried out. The vehicle model has been excited by an unknown disturbance z_k at each wheel which consequently influenced the roll acceleration of the car body and leads to a sense of ride comfort. To generate comparable values the spectrum for the whole maneuver is regarded in Fig. 5.

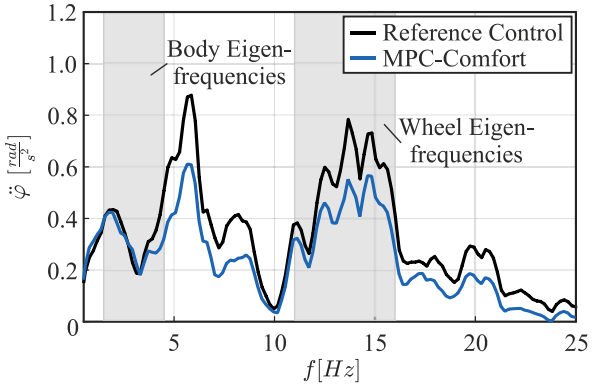

Fig. 5. Roll acceleration spectrum for the compared variants: Reference control and MPC-Comfort with $n_p = 10$

Obviously, almost throughout the whole frequency range the amplitudes were decreasing. Particularly, that is caused by two main factors. Firstly, the required forces were generated by both actuators coincidently which leads to lower required actuator angles and therefore a faster adjustment of the desired angle. Secondly, the controlled systems' behavior is known throughout the whole prediction horizon, so that oscillations of the body or the wheels, which are not controllable due to limited actuator dynamics, are almost eliminated within the optimization.

The huge variability of the MPC allows to analyze several variations of the matrices Q, R or the influence of the prediction horizon. The latter has been increased from $n_p = 10$ to $n_p = 50$ which obviously provides a larger time span of the future systems' behavior. Simulation results confirm that the roll acceleration is even increasing by that. A reason for the increase is the unknown road disturbance which can only be observed for the current time step k. The road disturbance input in the optimization is not changing for every following step. This generates an increasing error as the controlled system excitation and the assumed excitation in the optimization model are deviating. The results are displayed in Fig. 6. Additionally, the Delta Input Blocking strategy from section 3.4 is compared. This shows only smaller deviations as up to 3 Hz the amplitudes were decreasing and increasing between 3 Hz and 7 Hz.

The advantage of *MPC-DIB* is a hugely reduced computational time as the dimensions of the matrices within the optimization are decreasing. The presented control variants were tested with a *dSPACE* realtime system and an AMD Opteron CPU @ 2.8

GHz. By that, not only the influence on the ride comfort could be analyzed but also the required computation time.

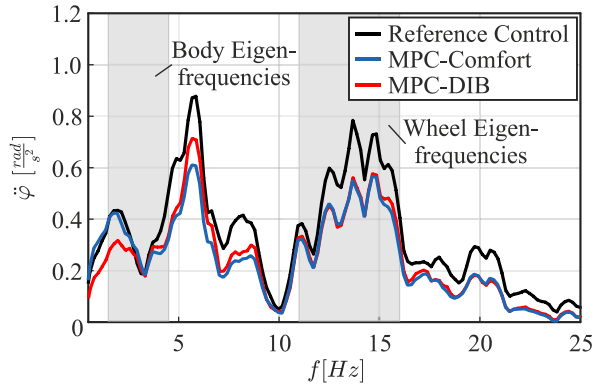

Fig. 6. Roll acceleration spectrum for the compared variants: MPC-Comfort and MPC-DIB with $n_p = 50$

In order to analyze the real-time capability, Fig. 7 shows the respective calculation times of the model predictive roll stabilization with a prediction horizon of $n_P = 10$ and $n_P = 50$. Therefore, the Delta Input Blocking described in Section 3.4 was used to increase the receding time horizon by a factor of 5 with the same number of optimization variables. It becomes clear that the numerical optimization of the actuating variables with both control strategies is performed below the required sample time of 2.5 ms and thus both approaches can be executed in real-time. Although the number of optimization variables is identical for both methods, it is noticeable that the use of a larger prediction horizon leads to a significant increase in computational effort. This can be explained by the complexity of the optimization problem to be solved, which is directly influenced by the choice of the prediction time. In addition, the distribution of the measurement data shows that the calculation times exhibit only a small dispersion. Thus, it could be verified by measurement data that both optimization-based control approaches can be performed within the available calculation time. Especially in the case of large prediction horizons, this can only be ensured by applying the presented Move Blocking strategy.

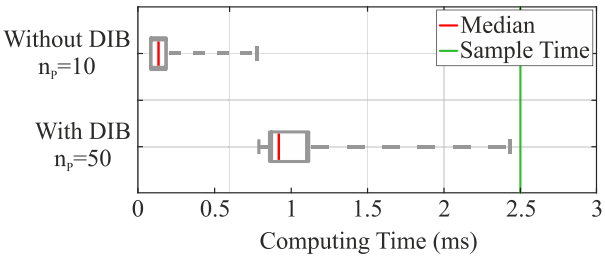

Fig. 7. Computing times of the MPC-based roll stabilization

5. CONCLUSION

This paper presents a new implementation of an MPC for disturbance compensation with an active chassis control system in a vehicle. Simulation study shows that respecting the limitations and formulating a corresponding optimization problem leads to an improved ride comfort. The prediction horizon influences the result hugely. The aim is to set the horizon as small as possible. The results confirmed that for a horizon of n_p=50, which is very large, it is still real-time capable if using Delta Input Blocking. Nevertheless, we propose that in future works n_p=10 or even less should be analyzed. In combination with *DIB* the computational time will be clearly short.

REFERENCES

Adamy, J. (2009). *Nichtlineare Regelungen*, Springer Verlag.

Biegler, L. T., Schmid, C. (1993). Reduced hessian successive quadratic programming for realtime optimization. *IFAC Advanced Control of Chemical Processes*, 173 – 178.

Cagienard, R., Griederer, P., Kerrigan, E. C., and Morari, M. (2007). Move blocking strategies in receding horizon control. *Journal of Process Control*, 17, 563-570.

Canale, M., Milanese, M., Novara, C. and Ahmad, C. (2006). Semi-active suspension control using fast model predictive control. *Control Systems Technology, IEEE Transactions*. Vol. 14. Nr. 6. 1034 – 1046.

Cho, B. (1999). Active suspension controller design using MPC with preview information. *Journal of Mechanical Science and Technology*. Vol. 13, 168 – 174.

Cho, B., Ryu, G., and Song, S.J. (2005). Control strategy of an active suspension for a half car model with preview information. *International Journal of Automotive Technology*. Vol. 6. 243–249.

Giorgetti, N., Bemporad, A., Tseng, H. E., Hrovat, D. (2006). Hybrid model predictive control application towards optimal semi-active suspension. *International Journal of Control*, Vol. 79. Nr. 5. 521–533.

Göhrle, C. (2013). Model Predictive Control of semi-active and active suspension systems with available road preview. *European Control Conference ECC*.

Illg, I., Freuer, A., Eisenbarth, M., Nareyko, G., Koch, T. (2018). Control strategy for electromechanical active roll stabilization, *18. Internationales Stuttgarter Symposium*, 363 – 376.

Ilmer, S. (2019). *Aufbau und Optimierung einer echtzeitfähigen modellprädiktiven Regelung für ein aktives Wankstabilisierungssystem*, Masters Thesis, University of Paderborn.

Koletzko, C. (2008). *Untersuchung des Einflusses von Verstelldämpfern auf das Wankverhalten von PKW unter Berücksichtigung einer aktiven Wankstabilisierung*, PhD Thesis, TU München.

Maciejowski, J. M. (2002). *Predictive control with constraints*. Pearson Education Limited.

Nareyko, G., Koch, T., Trächtler, A. (2019). Model predictive control of an active roll stabilization system, Autoreg 2019, 245 – 255.

Nguyen, M. Q., Canale, M., Sename O., Dugard L. (2016). A Model Predictive approach for semi active suspension control problem of a full car. *55th IEEE Conference on Decision and Control (CDC)*. Las Vegas.